Energy-dependent in-situ small-angle x-ray scattering study of nano-ceramics

Winter, Rudolf; Le Messurier, Daniel; Martin, Christopher M.

Publication date:
2006

Citation for published version (APA):
Winter, R., Le Messurier, D., & Martin, C. M. (2006). *Energy-dependent in-situ small-angle x-ray scattering study of nano-ceramics*. http://hdl.handle.net/2160/205

submitted to Cryst. Rev., 060119

Energy-dependent in-situ small-angle x-ray scattering study of nano-ceramics

RUDOLF WINTER*†, DANIEL LE MESSURIER† and CHRISTOPHER M. MARTIN‡

†Materials Physics, University of Wales Aberystwyth, Penglais, Aberystwyth SY23 3BZ, Wales

‡CLRC Daresbury Laboratory, Warrington WA4 4AD, England

*Corresponding author. Email: ruw@aber.ac.uk

Abstract

Energy-dependent small-angle x-ray scattering (SAXS) measurements near the Zr-*K* absorption edge of a nano-scale alumina-zirconia-silicate ceramic are reported. The *in-situ* experiments cover the temperature range from 250°C to 725°C, during which the sol-gel prepared nano-particles consolidate and the glass matrix phase begins to soften, leading to a compaction of the ceramic. The dominant scattering mechanism changes from a surface-fractal type to a mass-fractal type linked to direct contact areas between nano-particles and matrix. The energy-dependent data identify the zirconium-bearing phase as dominant in the high-q range. The experimental data are placed in the context of recent advances in *in-situ* anomalous small-angle x-ray scattering (ASAXS) and some experimental problems and solutions of near-edge scattering are discussed.

Keywords: Small-angle x-ray scattering, Anomalous small-angle x-ray scattering, Nano-ceramics, Refractories, Resonant scattering

1 Introduction

Small-angle scattering provides information on a material's structure on a length range beyond the atomic scale and up to a few hundred nm. As small-angle x-ray scattering (SAXS) maps electron density, it combines well as a technique with nuclear magnetic resonance (NMR), which is also a probe of electron density, but on the atomic scale.

Anomalous small-angle x-ray scattering (ASAXS) enhances the information that can be gained from SAXS by introducing a chemical, element-specific contrast, which modifies the standard electron density contrast obtained in normal SAXS experiments. This technique has the potential to help understand complex materials better, but its complexity means that it has so far not been used routinely in *in-situ* experiments. In this paper, we will review ASAXS and its *in-situ* applications as reported in the literature and present some data from a recent *in-situ*

near-edge SAXS experiment we did at beamline 6.2 at Daresbury.

Alumina-zirconia ceramics are widely used in industry as refractories and as catalyst supports. Nano-structured variants are particularly important as thermal barrier coatings, where careful engineering of the nanoscale structure can increase the mechanical strength significantly[1], and as bulk catalyst supports with a particularly large surface area. We have also used a nano-scale analogue of a commercial furnace refractory to study corrosion mechanisms in glass melting furnaces[2] along with *in-situ* NMR of glass melting kinetics[3].

These nano-ceramics consist of sol-gel prepared alumina and zirconia nanoparticles embedded in a silica-rich sodium silicate glass matrix. The corrosion mechanism is based on leaching of the glass phase followed by mechanical abrasion of the granular zirconia and alumina phases. The resilience of the refractory depends crucially on how well the grains are bonded to the matrix, *e.g.* by diffusion of Na^+ across the grain interfaces and reactive sintering. It also depends on the shape of the particles; oblong particles and whiskers are more likely to withstand the mechanical effect of the contact with the moving batch.

2 Anomalous Small-Angle Scattering

Anomalous scattering is the chemical contrast enhancement that occurs around the absorption edge of a probe element due to the resonance between scattering and absorption[4]. In a small-angle scattering experiment dealing with a heterogeneous material, the contrast between the different phases is usually governed by the difference in electron density. In an idealised material consisting of two types of particle densely packed within a matrix (cf. Fig. 1), the total scattered intensity is due to the scattering from the interfaces of either particle with the matrix. The intensity is proportional to the square of the scattering factor (*i.e.* the electron density difference):

$$I \propto (\Delta\rho)^2 \qquad . \tag{1}$$

Near the edge, a complex correction, $f' + \mathrm{i}f''$, is applied to the scattering factor to account for this resonance:

$$I \propto (\Delta\rho + f' + \mathrm{i}f'')^2 = (\Delta\rho)^2 + 2\Delta\rho f' + \left[(f')^2 + (f'')^2\right] \quad . \tag{2}$$

The first term is the non-resonant or normal contribution, which is independent of x-ray energy, but the cross (2nd), and resonant (3rd) terms have a characteristic energy dependence near the edge, which originates from the energy dependence of f' and f'' (cf. Fig. 2). Although the cross and resonant terms are small compared to the non-resonant contribution, they give rise to a chemical contrast if the probe element is inhomogeneously distributed about the different phases in the material. The resonant term relates to the distribution of the phase containing the edge element and the cross term represents correlations between the phases that contain the edge element and those phases that do not.

If SAXS experiments are carried out away from the edge (*i.e.* non-resonant only) and at two energies within the dip of f', then eq. (2) can be solved and the distribution of the labelled phase can be separated. In practice, it is better to use more than three energies because the resonant and cross terms are small and the solution is improved if the system of equations is over-determined.

Usually, all energies are chosen below the actual edge position in order to avoid excessive fluorescence. However, fluorescence can be corrected for if the incoming beam spectrum is known or the scattered intensity tails off to virtually zero in the high-q limit, so that the fluorescence level, which is supposed to be angle independent, can be regarded as the fluorescence contribution.

There is only a small number of ASAXS studies reported in the literature so far, and even fewer attempt to monitor materials *in situ* while varying a process parameter. Systems that have been investigated by ASAXS so far are concerned with phase separation in alloys[5, 6], distribution of counter-ions in polymer-coated core-shell particles[7], and porosity of catalyst supports[8]. The only *in-situ* stud-

ies so far are a kinetic study of an organometallic reaction leading to the formation of nano-particles[9], degradation of an electrocatalyst in operation[10] (both at room temperature) and phase separation kinetics in an alloy at moderate annealing temperatures[11].

Most of the previous ASAXS studies do not attempt to make full use of the potential inherent in eq. (2) to separate the cross term, which contains the correlation between the probe and the remaining scatterers, from the self term, which relates to the autocorrelation of the probes themselves, *i.e.* the pattern that one might expect if the phase containing the probe was in an otherwise perfectly index-matched environment. In order to solve eq. (2), measurements at a great deal more than three energies are required, and in addition to the usual corrections, the data need to be corrected for fluorescence, the width of the beam spectrum, and any chemical shifts of the edge occurring during an *in-situ* experiment[12].

3 Experimental

The nano-particles for our *in-situ* experiment were prepared by a water-based sol-gel technique[13, 14] using $AlCl_3$ and $ZrCl_4$. The Al:Zr ratio was varied, but all data shown here relate to the samples, where the molar Al:Zr ratio is 1:9. A sodium silicate glass was made from Na_2CO_3 and SiO_2 (1:3 by molar ratio) by melting at 1 300°C for 2 hours and a further half hour at 1 350°C and 1 400°C each. The glass was then crushed and mixed with the nano-powder mixture in a ratio of 1:1 by weight.

The SAXS experiments were carried out at beamline 6.2 at Daresbury. The beamline is equipped with a tunable Si(111) monochromator with horizontal and vertical focussing. The x-ray energy can be adjusted in steps of 1 eV, and the upper limit of energies available on the beamline is near 18 keV[15]. A one-dimensional Rapid-2 detector was used at a camera length of 4 m. The powdered samples were pressed into pellets 13 mm in diameter and about 0.25 mm thick; these were mounted into

a resistance-heated furnace with Mylar windows. In-situ experiments were conducted in a range 250°C to 725°C in steps of 25 K. Each temperature step took 17 minutes, comprising a 2 min temperature ramp, 3 min equilibration time, 5 min data acquisition at 18.02 keV and 18.05 keV (corresponding to the first XANES maximum and minimum post-edge, respectively) and 2 min data acquisition at 17.98 keV (pre-edge).

The accurate position of the Zr-K absorption edge was determined by scanning the edge before heating began. For comparison, a thin foil of zirconium metal was also edge-scanned (cf. Fig. 3). There is a chemical shift of about 8 eV between the metal reference and the oxide contained in our samples due to the different electron density in the two materials (chemical shift). In addition, there is also a chemical shift of about -3 eV in the edge position between the raw samples and the heated ones at the end of the *in-situ* experiment. From the resonance curve in Fig. 2 it is clear that the shift during the experiment needs to be corrected for, *i.e.* the x-ray energy has to be adjusted in line with the shift of the edge to maintain in the same relative position on the resonance curve. This would require frequent and accurate edge scans at each temperature step. As this was impractical at the time, we resorted to comparing pre- and post-edge scattering patterns, where the contrast variation is smaller but constant.

All scattering patterns are transmission corrected by evaluating the readings of two ion chambers before and after the beam passes through the furnace. At all three energies, fluorescence has to be taken into account since at least part of the beam spectrum is above the absorption edge. To this end, the run-out of the patterns at high q is interpreted as fluorescence-only, and all patterns are shifted vertically to coincide in this limit as indicated by the horizontal line in Fig. 4. The usable q window is therefore in the range from $0.15\,\mathrm{nm}^{-1}$ to $4\,\mathrm{nm}^{-1}$.

4 Results

Some of the scattering patterns obtained at 17.98 keV are shown in Fig. 4. The pattern at 250°C, which is identical to the room temperature pattern of the raw material, is fairly featureless with a slope near 2. As the temperature increases, a shoulder emerges in the higher-q range, which is sufficiently distinct at 350°C to determine a Guinier radius of about 0.6 nm. As the temperature continues to increase, this shoulder grows and shifts gradually to the left. At 625°C, the length scale of the scattering object associated with this shoulder has increased to 2.3 nm, and a plateau forms to the left of the slope. As the temperature rises further, the crossover between slope and plateau moves further to the left, and by 750°C, the Guinier radius becomes so large that only the sloping section remains to be observed. The exponent of the power law representing the slope increases from near 2 to 4 as the shoulder appears and then reduces again to a value near 3 as the shoulder moves towards the low-q end of the accessible q range.

The scattering patterns at 375°C just below and just above the Zr-K edge are shown in Fig. 5. At this temperature, the shoulder in the pattern is well established and it is straightforward to determine a Guinier radius. From the direct comparison of the two patterns (after adjusting the fluorescence level) it is obvious that the slope on the high-q side is steeper in the pre-edge pattern. On the other hand, there is little difference in the shape of the curves towards the low-q end of the range. The total scattered intensity is lower above the edge due to the fact that the sample as a whole is more absorbing. The difference pattern generally follows the shape of the pre-edge data set except for the area around $q \approx 2\,\mathrm{nm}^{-1}$, where the two curves approach each other more closely, indicating that the zirconium-bearing phase contributes more strongly in this region.

5 Discussion

The slopes of the scattering patterns are well below 4 almost throughout. This indi-

cates that the scattering objects are irregular units rather than distinct particles with a smooth surface, for which a slope of 4 is expected[16]. At the beginning, the samples consist of a powder mixture of large glass particles and nanometre-scale alumina and zirconia particles. We can expect the nano-particles to fill in gaps between the large glass grains. The contrast at this stage will arise from the difference in electron density between alumina, zirconia, and glass on the one hand and air on the other as the direct contact area between grains is small. As a consequence of the compressed q window at the relatively high x-ray energy of 18 keV, the focus is on very small-scale scatterers. The untreated sol-gel nano-particles have a rather fuzzy appearance as a consequence of the rapid precipitation from the sol. Once some thermal energy is provided, they can reconstitute as more defined objects, causing the appearance of a shoulder, from which in turn a Guinier radius can be obtained. This Guinier radius is only 0.6 nm at first, so the distinct core of such a particle still contains only a few atoms. As the temperature rises, the glass begins to soften. Once the dilatometric softening point (about 500°C) is reached, deformation occurs on the time scale of the experiment, and the contrast changes from particle-air to that arising from direct contact between glass and nano-particles. A detailed analysis of the evolution of the slope of the scattering patterns pre- and post-edge supports this mechanism[17]. When interpreting the data in terms of a fractal model[18], the structure evolves from a surface-fractal to a mass-fractal type, indicating that the contrast changes from being dominated by particle surface scattering to interface scattering.

6 Conclusions and Outlook

The purpose of this study was to show that the contrast variation near an absorption edge provides enough additional information to enable the study of the medium-range structure of complex materials subject to chemical and physical processes on the time scale of the experiment. At the same time, the limitations

which the technique imposes and possible ways to overcome them were also to be determined.

It is clear that the added complexity is a price worth paying if a material consists of several phases whose scattering contrast is expected to be similar. If the contrasts are subject to change, *e.g.* if (as in our case) the material compacts during a process or if it undergoes chemical reactions, then the additional information gained from anomalous or near-edge scattering will provide extra information that may help to piece together the processes involved.

In-situ ASAXS experiments rely on fast tunable monochromators and, depending on the time scale on which processes are to be monitored, fast detectors. The ability to tune the monochromator within a few seconds during an *in-situ* experiment is absolutely crucial, because doing separate runs with separate but supposedly identical samples opens up the possibility of artifacts because the conditions in the two runs may not be exactly identical. Beamline 6.2 at Daresbury, along with a few others, satisfies this requirement.

During the experiment, care needs to be taken to trace the exact position of the absorption edge if any chemical shifts arise. These may be due to chemical reactions or even simply thermal expansion. Frequent edge scans have to be incorporated into the schedule of any *in-situ* experiment.

A major drawback of experiments at high energies is the resulting compression of the observable q scale. In our experiment, for example, the q range covered was from $0.15\,\mathrm{nm}^{-1}$ to $4\,\mathrm{nm}^{-1}$ at 18 keV. With the same camera length and detector, we would have covered $0.06\,\mathrm{nm}^{-1}$ to $1.8\,\mathrm{nm}^{-1}$ at the more usual 8 keV, which would have allowed us to observe sintering as well as nucleation and compaction of our material[2]. Longer camera lengths are therefore extremely desirable if available. Another side effect of the higher energy is that most beamlines are well outside their optimum brilliance, which may cause a problem if count rates are an issue,

e.g. if fast kinetics are to be studied.

Finally, the occurrence of fluorescence not just above, but near, the absorption edge is an important point to consider. The accurate beam spectrum at the relevant energy is required to correct for fluorescence quantitatively. Failing that, it is crucial that the high-q limit is free from any scattering contribution, so that it can be used as a measure of fluorescence.

In-situ anomalous and near-edge scattering is useful for the study of kinetic problems involving complex materials. The technique has been applied successfully to polymer kinetics, electrochemical problems, annealing of metals, sol-gel precipitation, catalysis, and now the compaction of nano-ceramics. With the lessons learnt, we hope to be able to extend this work to *in-situ* experiments of sintering of nano-ceramics and other high-temperature applications.

Acknowledgements. We would like to thank Chiu Tang, now at Diamond Light Source and station scientist at Daresbury at the time. DLM would like to thank Pilkington plc and the Engineering and Physical Sciences Research Council for a PhD studentship from the Collaborative Awards in Science and Engineering scheme. Beamtime was awarded by the Council of the Central Laboratory of the Research Councils.

References

[1] J.R. Nicholls, R.G. Wellman, M.J. Deakin, Mater. High. Temp., **20**, 207 (2003).

[2] D. Le Messurier, N. Sissouno, A.R. Vearey-Roberts, S. Evans, D.A. Evans, R. Winter, Mater. Sci. Technol., **20**, 975 (2004).

[3] A.R. Jones, R. Winter, P. Florian, D. Massiot, J. Phys. Chem. B, **109**, 4324 (2005).

[4] G. Materlik, C.J. Sparks, K. Fischer (Editors), *Resonant Anomalous X-ray Scattering* (North-Holland, Amsterdam, 1994)

[5] W. Liu, W.L. Johnson, S. Schneider, U. Geyer, P. Thiyagarajan, Phys. Rev. B, **59**, 11 755 (1999).

[6] A. Hoell, A. Wiedenmann, F. Bley, J.P. Simon, A. Mazuelas, P. Boesecke, Scripta Mater., **44**, 2 335 (2001).

[7] B. Guilleaume, M. Ballauff, G. Goerigk, M. Wittemann, M. Rehahn, Colloid Polym. Sci., **279**, 829 (2001).

[8] A. Bóta, G. Goerigk, T. Drucker, H.G. Haubold, J. Petró, J. Catal., **205**, 354 (2000).

[9] K. Angermund *et al.*, J. Phys. Chem. B, **107**, 7 507 (2003).

[10] H.G. Haubold, X.H. Wang, G. Goerigk, W. Schilling, J. Appl. Cryst., **30**, 653 (1997).

[11] G. Goerigk, H.G. Haubold, W. Schilling, J. Appl. Cryst., **30**, 1 041 (1997).

[12] M. Patel, S. Rosenfeldt, M. Ballauff, N. Dingenouts, D. Pontoni, T. Narayanan, Phys Chem Chem Phys, **6**, 2 962 (2004).

[13] G.B. Prabu, D.L. Bourell, NanoStruct. Mater., **6**, 361 (1995).

[14] A.J.A. Winnubst, W.F.M.G. Zevert, G.S.A.M. Theunissen, A.J. Burggraaf, J. Mater. Sci. Eng. A, **109**, 215 (1989).

[15] C.C. Tang, C.M. Martin, D. Laundy, S.P. Thompson, G.P. Diakun, R.J. Cernik, Nucl. Instrum. Meth. Phys. Res. B, **222**, 659 (2004).

[16] J.S. Pedersen, Adv. Colloid Interf. Sci., **70**, 171 (1997).

[17] D. Le Messurier, R. Winter, C.M. Martin, , , (submitted).

[18] S.K. Sinha, in: *Complementarity Between Neutron and Synchrotron X-ray Scattering*, edited by A. Furrer (World Scientific, Singapore, 1998), p. 251

Figure Captions

Fig. 1: Schematic of the three contributions to the scattering contrast near an absorption edge of an element contained in the phase represented by the black spheres. The normal scattering contrast combines electron density difference between both black and grey particles and the matrix, the resonant term represents the correlation of scatterers containing the edge element (solid lines), and the cross term contains correlations between the phases that contain the edge element and those that don't (broken lines).

Fig. 2: Resonant correction of the atomic scattering factor near an absorption edge (Zr-*K* in this case). The real part (f',circles) shows a sharp dip at the edge, while the imaginary part (f'', diamonds) increases suddenly.

Fig. 3: Zr-*K* edge scans of zirconium foil and zirconia-alumina-silicate mixture. A chemical shift of 8 eV arises due to the different electron densities. A further chemical shift of -3eV is observed during the *in-situ* experiment. The arrows indicate the energies at which *in-situ* SAXS patterns were recorded.

Fig. 4: Scattering patterns at 17.98 keV at 250°C, 350°C, and 625°C. The horizontal line indicates the fluorescence level to which all patterns are normalised. Guinier radii are obtained from the shoulder where possible. The three dashed lines in the top right corner indicate slopes of 2, 3, and 4.

Fig. 5: Pre- and post-edge scattering patterns (obtained at 17.98 keV and 18.02 keV, respectively) at 375°C. The difference pattern emphasises those areas where scattering is dominated by the Zr-bearing phase. The vertical dashed line indicates the limit of confidence in the accuracy of the fluorescence correction.

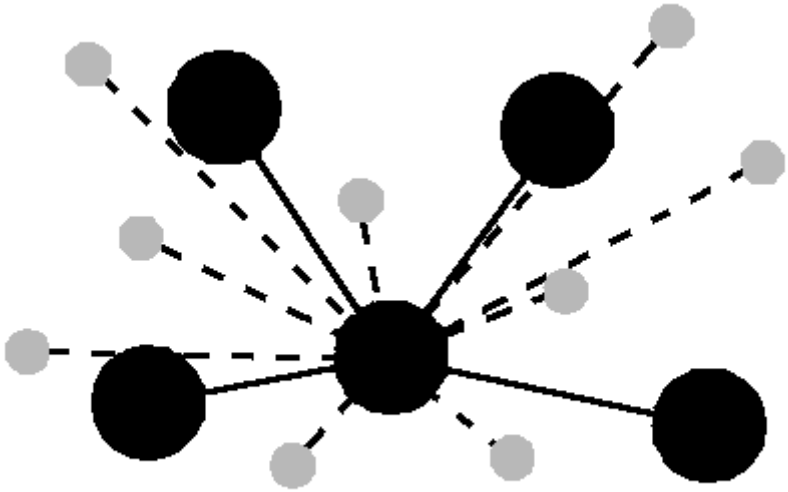

Fig. 1

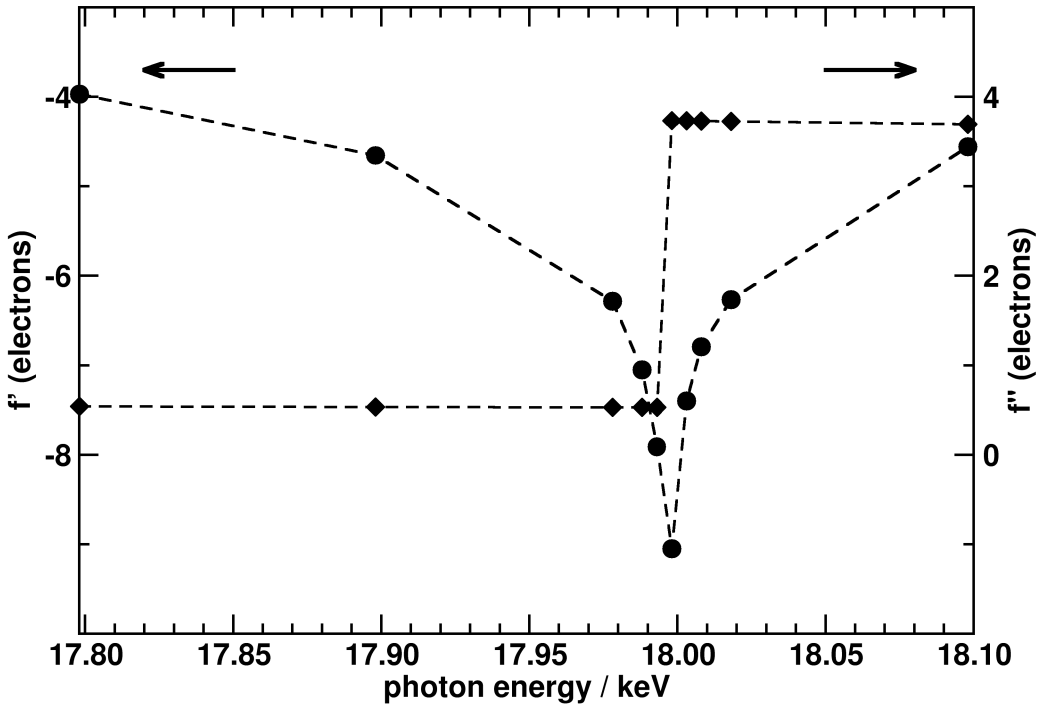
f' (electrons)
f'' (electrons)
-4
-6
-8
4
2
0
17.80
17.85
17.90
17.95
18.00
18.05
18.10
photon energy / keV

Fig. 2

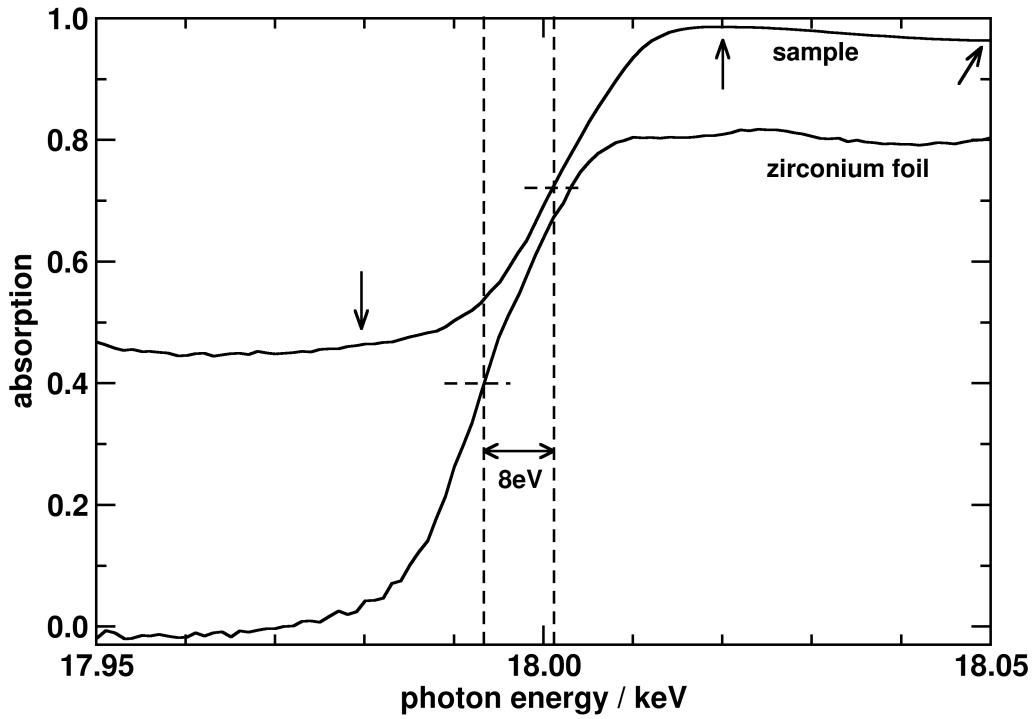
1.0
0.8
0.6
0.4
0.2
0.0
absorption
sample
zirconium foil
8eV
17.95
18.00
18.05
photon energy / keV

Fig. 3

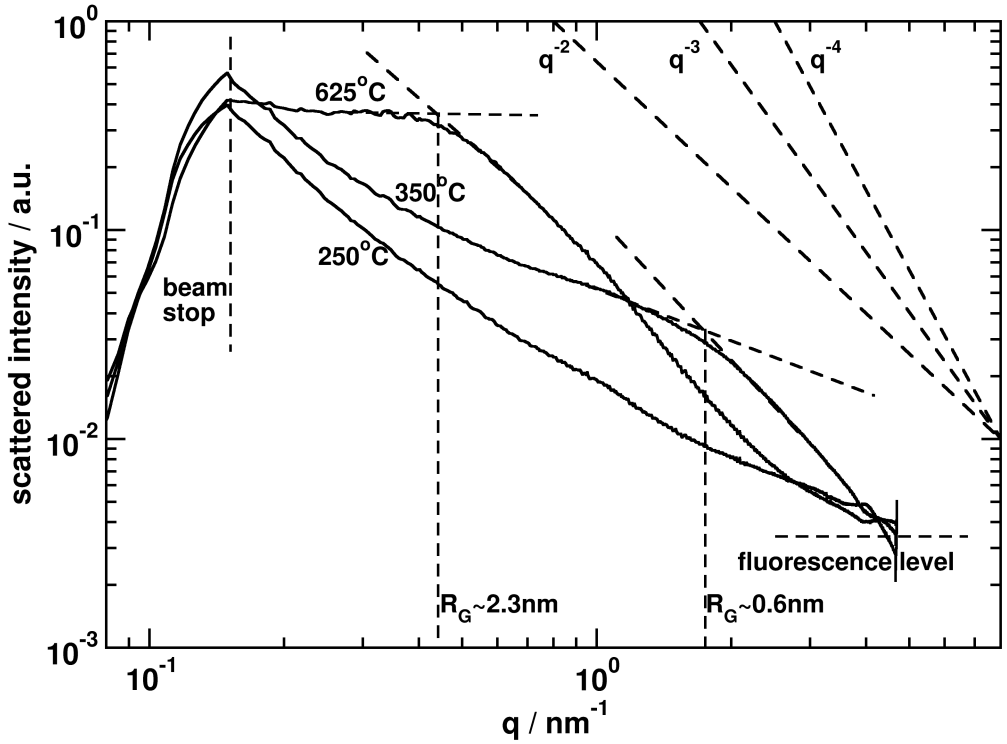
scattered intensity / a.u.
q / nm^{-1}
10^{0}
10^{-1}
10^{-2}
10^{-3}
10^{-1}
10^{0}
q^{-2}
q^{-3}
q^{-4}
625°C
350°C
250°C
beam stop
R_G~2.3nm
R_G~0.6nm
fluorescence level

Fig. 4

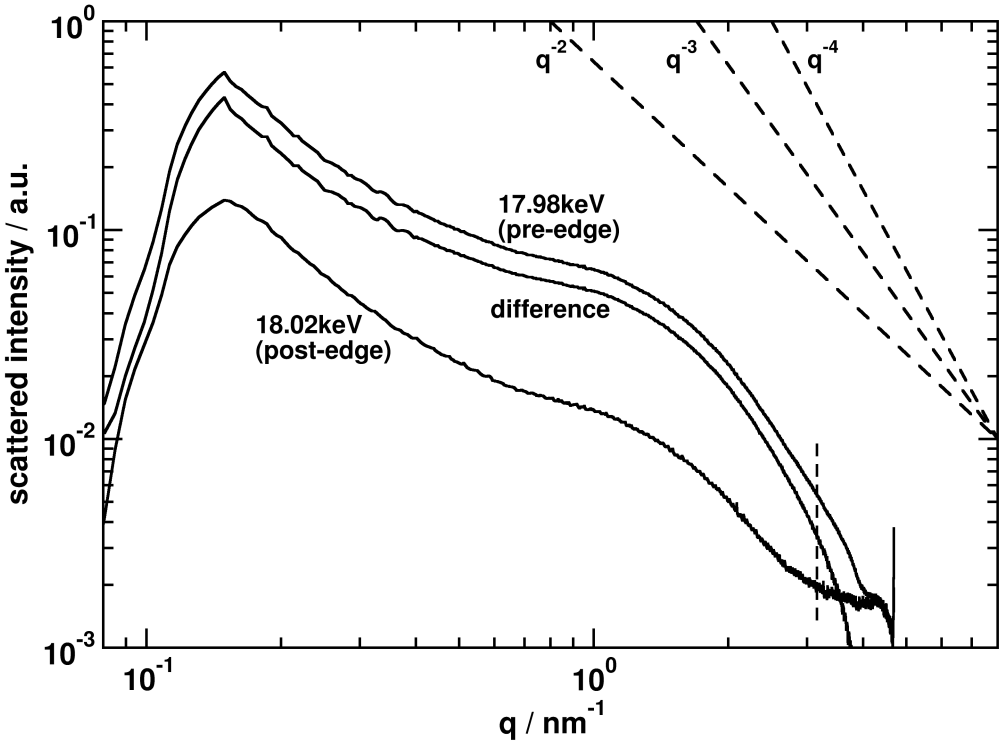

Fig. 5

rw/060119